INTERNATIONAL JOURNAL OF
COASTAL & OFFSHORE ENGINEERING
IJCOE Vol.1/No. 2/Summer 2017 (27-39)

Available online at: http://ijcoe.org/browse.php?a_code=A-10-56-1&sid=1&slc_lang=en

Tsunami Assessment for Inundation Risk Management at Chabahar Bay Facilities in Iran

Mahmood Reza Akbarpour Jannat[1*], Ehsan Rastgoftar[2], Toshyuki Asano[3]

[1] Corresponding author: Iranian National Institute for Oceanography and Atmospheric Science (INIOAS), Ocean Engineering and Technology Research Center, Tehran, Iran; akbarpour@inio.ac.ir*
[2] Iranian National Institute for Oceanography and Atmospheric Science (INIOAS), Ocean Engineering and Technology Research Center, Tehran, Iran; ehsan_rg8@yahoo.com
[3] Dept. of Ocean Civil Engineering, Kagoshima University, Japan; asano@oce.kagoshima-u.ac.jp

ARTICLE INFO

Article History:
Received: 29 Aug. 2016
Accepted: 10 Jul. 2017

Keywords:
Makran Subduction Zone
Earthquakes
Tsunamis
Numerical model
Inundation

ABSTRACT

In this study two numerical models, one a regional generation and propagation model and the other an inundation model, have been applied to the problem of examining the impact that a large, locally generated tsunami could have on Chabahar Bay facilities in Iran. To achieve a realistic outlook of tsunami hazards in the area, the generation, propagation and interaction of tsunami waves with Chabahar Bay coasts is being numerically modeled for specific events. The modeling is performed using the numerical code which solves the nonlinear Boussinesq wave equations. Results of numerical simulations performed in this study considering past tsunami occurrence records indicate that the multipurpose Chabahar Port is expected to experience the tsunami events with heights ranging between 8 to 10 meters. The model gives approximately the observed maximum area of flooding of Chabahar City. The large and small amount of fooding of Chabahar city coasts, Iran from the 9.1 and 8.3 magnitude erarthquake achieved respectively and extensively flooding was reproduced by the numerical model. The effect of the tide was modeled and found to be small. The results of this study are intended for emergency planning purposes. Appropriate use would include the identification of evacuation zones. The results are used also to find a best configuration advice for the urban facilities in order to mitigate tsunami related risks, with positioning such facilities at the Western Cape of the bay.

1. Introduction

Makran Subduction Zone (MSZ) and Andaman-Nicobar- Sumatra Arc are two main tsunamigenic zones in the Indian Ocean which have detectable underwater seismic activities for causing tsunamis. There are many evidences based on historical reports and numerical modeling which show many tsunamis have been happened with different sources until 1945 in the MSZ (Ambraseys and Melville., 1982). The MSZ is the second murderous tsunami in the Indian Ocean and important source for large tsunamis, as we know from the magnitude 8.1 earthquake and tsunami that occurred there in 1945 with a death toll of about 4000 people (Pararas and Carayannis., 2006). Following the enormous Indian Ocean tsunami in December 2004 and menaced to more than 225,000 human live and leaving at least a million homeless was cause more serious consideration to this adventure in identifying the risks of vulnerability on different coasts around the world, mainly for marginal Indian Ocean countries (Geist et al., 2006).

Heck (1947) provided a list of global tsunamis generated from 479 BC to 1946, that some of them were relevant to tsunami incidences in the Arabian Sea and neighboring zones. Berninghausen (1966) collected another list of tsunami containing 27 tsunamis reported from areas adjacent the Indian Ocean which three events were from the west coast of India and the Arabian Sea. Page et al. (1979) as a significant tsunami valency, presented document for the recurrence of large magnitude earthquakes along the MSZ and predict the 1945 type earthquake can happen every about 150–250 years in eastern Makran. Other list gathered by Murty and Rafiq (1991) used a diversity of sources in the Indian Ocean region from 326 BC to 1974. Byrne et al. (1992) furthermore studied massive thrust earthquakes along the MSZ.

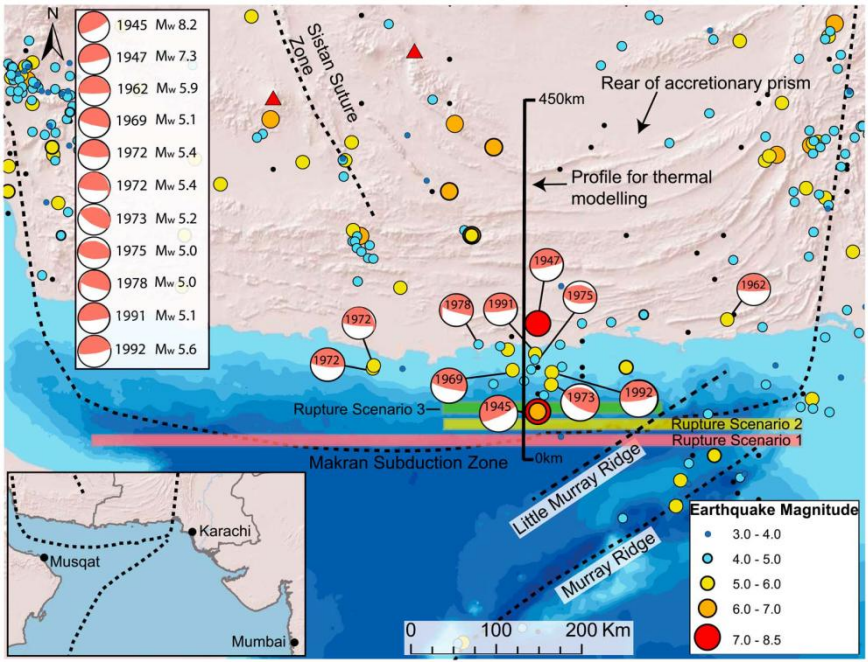

Figure 1. Location map of the Makran Subduction Zone and earthquakes (Smith et al. 2013)

The thermal modeling by Smith et al. (2013) indicates that M_w 8.7–9.2 earthquakes are thinkable in the seaward MSZ. These earthquakes and related tsunamis have important implications, specially for the neighbor coastlines of Iran, Pakistan, Oman, and India, whereas the Makran has not been formerly imagined a probable applicant for a Mw>9 earthquake. Fig. 1 illustrates location map of the MSZ and Earthquakes from post-1960 and pre-1960 published by Smith et al. (2013).

Chabahar Bay (CB), as the largest Iranian bay type semi-enclosed water basin, is located at the end of the North-Eastern coasts of the Gulf of Oman. Two major South-Eastern ports of Iran, namely, Chabahar Multi-purpose Port (CMP) and Konarak Fishing Port (KFP), are located in the South-East and South-West of the bay, respectively, engaged with fishery, marine transportation and oil terminals activities. In recent years, within the national development plans of Iran, major ongoing port construction activities have been undertaken for expansion of the CMP as a portal on the transit corridor into the Commonwealth of Independent States (CIS) countries. However, the certainty of tsunami occurrence is undeniable in the MSZ, and therefore any substantial investment in the development of the port facilities is contingent upon a thorough investigation of potential tsunami impacts.

There are several different methods for studying tsunami, such as paleotsunami data utilization, historic tsunami consideration, DART systems, tide gages and numerical simulation. Neetu et al. (2011) presented while there is document that the earthquake might have operated submarine mudslides in the MSZ (Byrne et al. 1992; Ambraseys and Melville 2005), other studies show that it is not essential to exert any other source such as mudslides to specify the tide-gauge data. Therefore, only numerical simulation of earthquake-induced tsunamis are focused in this paper. Tsunami behavior simulation using historical data and numerical modeling is still common due to low cost. Numerical simulation of tsunami is very important for comprehension past events and modeling future ones. Definition of the potential run-ups and inundation associated with tsunami by using numerical simulation is a useful and important tool, since data from past events are usually inadequate (Rafi and Mahmood 2010; Akbarpour et al. 2011; Rastgoftar et al. 2012; Heidarzadeh and Satake 2014).

Tsunami models can be used to simulate the past tsunamis and worst case scenarios for the tsunamigenic earthquakes to determine the impact on adjacent coast as well as on the away coasts. Tsunami evacuation maps and procedures can be created based on information from these probable worst case scenarios. To simulate possible tsunami scenarios from the MSZ (Fig. 1), information about the seismic deformation and mechanism of earthquake is necessary as an input to specify the initial deformation at the source and then calculate the tsunami life steps.

Tsunami generation in the regional model involves the represent of seafloor deformation by a major strength earthquake. However, vertical seafloor deformation (both uplift and subsidence) describes the initial amplitude of the tsunami. Several different models exist that can compute deformation patterns based on assumptions the slip, depth, length, width, and dip angle of the earthquake fault plane. The application of numerical modelling to determine the potential run-ups and relevant inundation from a local or distant tsunami prepares considerable information about the tsunami incident.

Hence, the procedure to appraise the tsunamis for the Chabahar Bay Facilities (CBFs) assessment can be separated into two parts as 'Verification of the fault

model concerning the numerical calculation' and 'Determination of the tsunami heights along with inundation area'. The impact associated with tsunami affects on a studying area can include several related phenomena such as water's rise and fall, floating materials and so on. For CBFs assessment, evaluation of water rise and fall is the most significant because the water rise and run-up of a tsunami may damage buildings and facilities on land and water receding for long time cause the problem of desalination systems.

In this study, a comprehensive numerical modelling study was accomplished for the generation, propagation, and flooding of tsunami waves with CB coasts, Iran. The flooding of CB by the tsunamis were simulated using the fully nonlinear Boussinesq equation code GEOWAVE including the friction effects. The regional model is first used to generate the tsunami at the source through several earthquake scenarios with their corresponding fault-plane parameter sets and propagate the tsunami to the input boundary of the inundation model, which can then perform the flooding computations. This study illustrates an approach to estimating the potential flooding of tsunamis along the Iranian coastline. Finally, it should be mentioned that this study represents the new effort at integrating seismology and oceanography to study locally generated tsunamis and inundation in CB, Iran.

2. Methodology

2.1. Numerical Model

Numerical modelling is an impressive approach to studying the events of tsunami, particularly for the future hazards. As yet, many numerical models have been modified or lately developed to impressively and carefully study the generation, propagation, run-up and inundation of tsunami. The achievement of tsunami studies depends on the combination of precise tsunami sources, an advanced tsunami propagation and finally inundation model. In this study, one of the tsunami models, GEOWAVE, is adopted to study the run-up and inundation of potential tsunami generated from MSZ.

GEOWAVE is a tsunami numerical model formed by merging the Tsunami Open and Progressive Initial Conditions System (TOPICS) with the Fully Nonlinear Boussinesq water wave model FUNWAVE (Grilli et al. 2007). In this work, GEOWAVE was validated with successful case studies of the 1945 Makran events. It simulates accurate run-up and inundation at the same time, using a slot technique. Wave breaking is also accounted with a dissipative breaking model acting on the wave front during shoaling or run-up. This model is able of studying the whole life range of tsunami including its generation, propagation, run-up and inundation. The model can use a larger grid resolution to simulate the propagation of tsunamis in the deep ocean and then convert to apply finer grid resolutions in coastal regions to calculate for the tsunami waves shortening because of the shallow water. Through the implementation of nested grids in this method, the computational and the numerical precision can be moderated. This model has been validated and has shown its satisfactory accuracy when compared to analytical solutions and experimental studies (Wei and Kirby 1995; Wei et al. 1995; Chen et al. 2000; Kennedy et al. 2000), and benchmark problems (Watts et al. 2003, 2005; Waythomas and Watts 2003; Day et al. 2005; Ioualalen et al. 2006; Grilli et al. 2007). This model has been successfully applied to study the propagation, run-up and inundation of several historical events including the 1946 Unimak, Alaska; the 1946 Skagway, Alaska and the 1998 Papua New Guinea (Watts et al., 1999) and indicated satisfactory achievements in comparison with either field or satellite observations and tidal gauge measurements. It has also been exerted to study the flooding and tsunami forces on structure.

In this study the effect of tsunami occurring at high-tide was modelled in some of the scenarios. It was approximated by adding a half the average tidal range of about 1.7 m for CB to the base water level.

The run-up is the major phase of tsunami modeling which the magnitude and effects of tsunami are defined based on the tsunami wave height and inundation areas. An inundation numerical model requires more computational resources like as coastal topography and hydrography than the typical propogation model. Hence, it is not reasonable to use an integrated model for simulation all of the tsunami phases. Instead, a hybrid method is usually used and run-up calculations are limited to areas where detailed study of the inundation process is needed.

The present numerical modelling of tsunami is performed in two distict global and local models. In the global model, the initial wave of tsunami is generated and then it propogates from MSZ to the coastlines. The local model which used when the waves reach to areas that have high significance for calculation of tsunami run-up. When the waves enter to the neighborhood of local models, the global model is stopped and the local model is begun. Free surface elevation and water velocities which are achived at the final time step of global model, are constrained to the local model as the initial conditions. As the stations have been almost located at the coastline, the recorded wave height can be assumed as run-up height. Fig. 2 shows the global and local domain of tsunami modeling.

The possible impact along the Makran Coast is assessed in more detail by selecting a series of numerical virtual tidal gages along the East–West Makran Coast. Virtual tidal gauges were deployed in the numerical models to path the arrival times of tsunami and the water surface oscillations for different

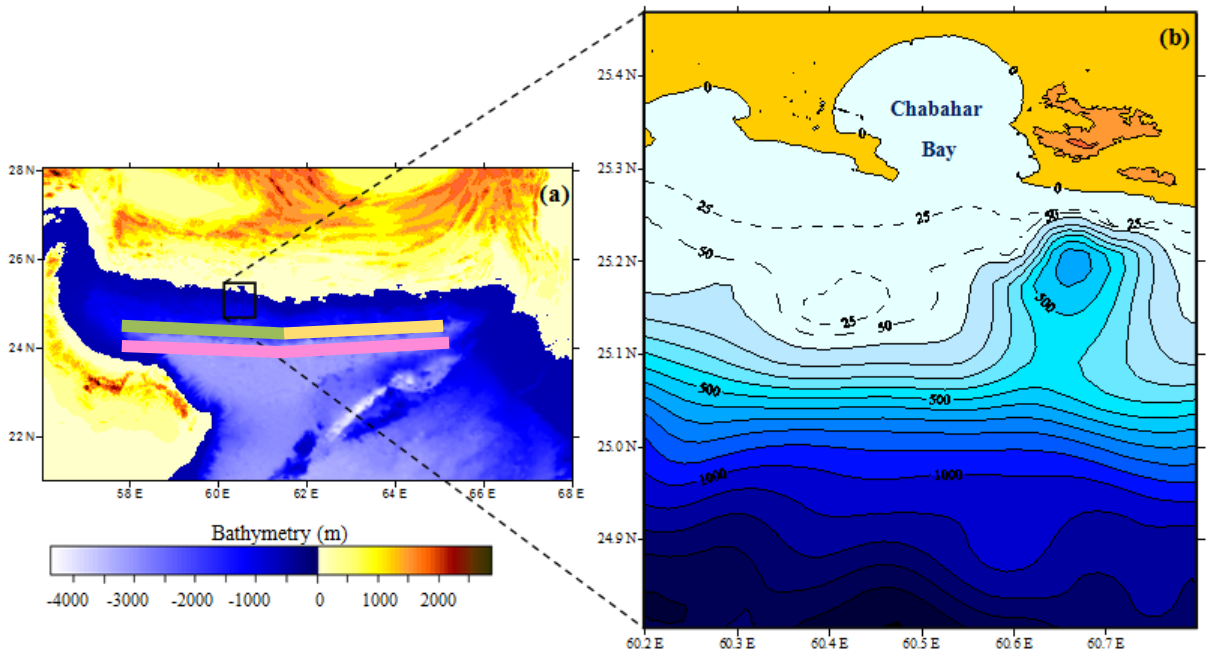

Figure 2. (a) Locations of bathymetric data and (b) depth contours used for coastal to construct numerical grid. Three tsunamigenic sub-regions in the MSZ used in this study as Western Makran (WM), Eastern Makran (EM) and Full length of Makran (FM) and are shown with olive green, light yellow and pink lines.

tsunami scenarios. The UTM coordinates and water depth of these virtual tidal gauges are given in Table 1 and Fig. 2. The virtual tide gauges measure the instantaneous sea water level relative to mean sea level.

Table 1. Locations of virtual tidal gauges

Gauge No.	Longitude (°E)	Latitude (°N)	Depth (m)
1	60.610	25.285	1.06
2	60.404	25.355	1.4
3	60.313	25.360	1.97
4	60.491	25.439	1.84

2.2. Model Grids Construction

It is obvious that as tsunami comes close to the coastal regions from the deep water, its wave length becomes shorter and the amplitude becomes larger because of the water shoaling in comparison with wave characteristics in the deep water. To describe this effect, two types of bathymetric and topographic data resolution (1 minute and 3 seconds) were implemented for the numerical models. The first type grids cover the entire region of Oman Sea, local fault zones where future earthquakes could generate tsunami potentially threatening the CB area with 1 minute grid resolution (Fig. 2). The second type grid covers the entire CB and a significant southwest area of the CB with 90 m grid resolution. The water depth in most regions of this grid domain is usually less than 20 meters (Fig. 2). This high resolution bathymetric and topographical data was achieved from Community Model Interface for Tsunami (ComMIT) database which approved by NOAA, and is used to obtain the applicable details of run-up and inundation in the CB area for possible tsunami events. The minimum depth parameter in the model is set to 0.1 m to bound the bottom friction near the CB coasts. The simulation of the tsunami generation and propagation through the Gulf of Oman to the CB was performed using a 1 minute grid of ocean depths. This equipped a appropriate input of wave characteristics for the modelling of the tsunami interaction with the CB on a 3 second grid. The consequent wave specification arriving at entrance of the CB was used to simulate the tsunami wave interaction with the bay, harbour and Chabahar town on a 90 m grid. Each grid was demonstrated by its height above or below sea water level.

2.3. Model Governing Equations Description

In this model, the fully nonlinear Boussinesq equations relying on the Wei et al. (1995) study, with various parameters implemented to consider bottom friction, breaking, and shoreline run-up effects proposed by Chen et al. (2000) and Kennedy et al. (2000) have been applied. The volume conservation and momentum equations are defined as follows,

$$\beta\eta_t + \nabla_h . M = 0 \quad (1)$$

$$u_{\alpha t} + (u_\alpha . \nabla_h)u_\alpha + g\nabla_h\eta + V_1 + V_2 + R_f - R_b = 0 \quad (2)$$

in which $\eta(x, y, t)$ is water surface elevation relative to the local mean depth $h(x,y)$; ∇_h is gradient in horizontal coordinates and M is depth-integrated horizontal volume flux which is given by Eq. (2). V_1 and V_2 represent dispersive effects and are given by Eq.(4) and Eq.(5) in

Grilli et al. (2007). R_b and R_f are forces related to the wave breaking and bottom friction, respectively, and are explained by Kennedy et al. (2000).

$$M = \Lambda\left[u_\alpha + \left(\frac{\mathcal{Z}_\alpha^2}{2} - \frac{1}{6}(h^2 - h\eta + \eta^2)\right)\nabla_h A + \left(\mathcal{Z}_\alpha + \frac{1}{2}(h-\eta)\nabla_h B\right)\right] \quad (3)$$

$$V_1 = \frac{\mathcal{Z}_\alpha^2}{2}\nabla_h A_t + \mathcal{Z}_\alpha \nabla_h B_t - \nabla_h\left[\frac{\eta^2}{2}A_t + \eta B_t\right] \quad (4)$$

$$V_2 = \nabla_h\left[(\mathcal{Z}_\alpha - \eta)(u_\alpha.\nabla_h)B + \frac{1}{2}(\mathcal{Z}_\alpha^2 - \eta^2)(u_\alpha.\nabla_h)A\right] + \frac{1}{2}\nabla_h[(B+\eta A)^2] \quad (5)$$

In Eq.(3), u_α is horizontal velocity at an elevation $\mathcal{Z}_\alpha$ taken to be $\mathcal{Z}_\alpha = -0.531h$, following Wei et al. (1995). A and B are functions of velocity given as follows,

$$A = \nabla_h . u_\alpha \quad (6)$$

$$B = \nabla_h . (h u_\alpha) \quad (7)$$

The factors β and Λ were implemented to simulate a porous beach method for calculation of run-up on dry shorelines. These factors are shown as follows;

$$\beta = \begin{cases} 1 & , \quad \eta \geq \mathcal{Z}^* \\ \delta + (1-\delta)e^{\lambda(\eta - \mathcal{Z}^*)/h_0} & , \quad \eta \leq \mathcal{Z}^* \end{cases} \quad (8)$$

$$\Lambda = \begin{cases} (\eta - \mathcal{Z}^*) + \delta(\mathcal{Z}^* + h_0) + \frac{(1-\delta)h_0}{\lambda}\left(1 - e^{-\lambda(1+\mathcal{Z}^*/h_0)}\right), & \eta \geq \mathcal{Z}^* \\ \delta(\eta + h_0) + \frac{(1-\delta)h_0}{\lambda}e^{\lambda(\eta-\mathcal{Z}^*)/h_0}\left(1 - e^{-\lambda(1+\eta/h_0)}\right), & \eta \leq \mathcal{Z}^* \end{cases} \quad (9)$$

$$z^* = \frac{-h}{1-\delta} + h_0\left(\frac{\delta}{1-\delta} + \frac{1}{\lambda}\right) \quad (10)$$

Here, h_0 is the porous layer depth. It must be deeper than depth of maximum wave rundown during a calculation. The selection of $\mathcal{Z}^*$ is explained by Kennedy et al. (2000). Here we use parameter values δ =0.08 and λ =25, according to the number of tsunami run-up events investigated by Watts et al. (2003), Day et al. (2005) and Grilli et al. (2007).

3. Determination of Tsunami Heights

3.1. Fault Models and Scenarios of Possible Tsunamis

According to the empirical formulas proposed by Wells and Coppersmith (1994) based on rupture parameters, we approximate a sensible earthquake source for the MSZ, in terms of magnitude and the seismic seafloor movement along about 1000 km of the MSZ. We refine this approximation by subsequent restricting the source and simulated tsunami to adjustment impressive aspects of associated magnitudes.

In this study, earthquake tsunami source is based on the half-plane solution for an elastic displacement with maximum slip (Okada, 1985). Thus, we specify an oblique planar fault of horizontal length *L* and width *W*, with centroid placed at latitude-longitude (x_e,y_e), and depth *d* of the earthquake at the centroid, and discretize it into many small trapezoids. The vertical displacement on the ocean floor at the fault is estimated by summing up contributions of point source elastic solutions, based on the actual depth of each trapezoid. The shear modulus μ will be supposed to be constant in this study. Okada's solution is performed in TOPICS, the tool that prepares the vertical seismic displacements as outputs, in addition the tsunami wavelength and tsunami period. The initial tsunami amplitude is specified as the minimum or maximum elevation initiated from the bottom seismic movement. The seismic moment M_0 ($\approx M_w$) is proportional to $\mu LW\Delta$, since a Gaussian slip distribution is supposed at the centroid (Grilli et al., 2007). The total seismic moment released with $\mu = 4 \times 10^{10}$ Pa.

We define nine separate tsunami sources for the nine segments. The earthquake parameters for each tsunami source are listed in Table 2. To detract the number of free parameters in Okada's sources, as well as the lack of precise geological data, we assumed all segments to have a rake angle 90° and a dip angle 3°, to rehabilitate the correct distances between seafloor aspects.

The width *W* of each segment, was firstly selected based on the empirical relationship of moment magnitude presented in Wells and Coppersmith report mentioned above. It is also represents the tsunami wavelength and hence is proportional to the tsunami period. The width was then repeatedly adjusted for the simulations to better estimate the major moment magnitudes based on seismic magnitudes obtained by W&C formula; so *W* generally attenuated from 70 km to 20 km based on M_w variations. According to the slip distributions requirement to satisfy moment magnitude and seismic magnitude relevance based on W&C formula, the earthquake depth *d* was fixed at 25 km, and maximum slip was specified to 3–14 m, except in Full length of Makran (FM) where it was increased to 25 m to model the severity of Makran. The maximum vertical seafloor subsidence or uplift (η_0) estimated by TOPICS for each source is listed in Table 2 and changes in the range -5.86;+8.43 m, which is proportional with the range of values approximated by the seismic models.

Table 2. Fault parameters of five scenario earthquakes

Magnitude (Mw)	Moment M_0 (N.m)	Area A(km^2)	Length L(km)	Width W(km)	Slip Δu(m)	η_0 (m)	Magnitude* (Mw)
9.1	$4.72x10^{22}$	35,000	500	70	25.0	-5.86;+8.43	9.11
8.7	$1.05x10^{22}$	25,000	500	50	14.0	-2.93;+4.15	8.68
8.3	$3.06x10^{21}$	12,000	300	40	8.50	-1.62;+2.30	8.32
8.0	$9.90x10^{20}$	6,000	200	30	5.50	-0.89;+1.26	8.00
7.5	$1.50x10^{20}$	2,000	100	20	3.00	-0.34;+0.49	7.50

* $M_w=2/3 \log_{10}(M_0)-6$

3.2. Verification of the Fault Model and the Numerical Calculation System

Recorded historical tsunami are considered to select generic tsunamis for studying region. In Iran, old tsunami records are not available because of the low technology accessible for the measurement at that time. Precise selection of the fault model parameters, bathymetry data and the numerical calculation model are essential for proper tsunami assessment. We can verify calculated tsunami heights with recorded and documented tsunami heights to evaluate the validity of the numerical calculation model.

The data of the Makran 1945 tsunami event, authorize us to validate the numerical model of the tsunami propagation. Because of the lack of persistent sea-level measurements of the tsunami, the sea-level observations of the Makran 1945 tsunami from the tide gauge at Karachi in Pakistan is persumed for numerical model validation. The maximum wave height of tsunami recorded at Karachi was 44 cm in which compatible with the existent numerical model that calculated 50 cm wave height at the same station. Compatible with the reports by Neetu et al. (2011) and Rajendran et al. (2008), the present model result indicates the wave height of 250 cm in Pasni.

3.3. Uncertainty Analysis

Because of the tsunami nature and resultantly difficulty to consider all the uncertainties quantitatively, uncertainties can be categorized as two types. Some uncertainties such as tsunami occurrence time which is called aleatory and someone such as tsunami source, fault position, dip angle or strike direction which is named as epistemic. Epistemic uncertainties can be scrimp through the application of the precise data and numerical modeling.

Uncertainty analysis can improve the accuracy of tsunami modeling, however the present study has not been performed in this conception. Resultantly, because of the significantly influence of tsunami source on the tsunami assessment, uncertainties related with tsunami source are interested in the present study (Table 3). Uncertainties associated with the tsunami sources are conducted as follows, (1) collecting the variety range of fault models parameters, (2) conducting a numerical modeling for each fault models mentioned above and (3) choosing the most critical scenario in each studying area as the most serious event on the studying site.

4. Results & Discussion

4.1. Tsunami Heights

The maximum simulated tsunami elevations above sea level are displayed in Fig. 3(a,b,c) with details given in Fig. 3(d,e,f,g) for M_w 9.1 tsunami source . The tsunami radiation patterns in Fig. 3 show high directionality, both because of the source length and in relation with the various seafloor features. To the south, tsunami propagation covers most of the Gulf of Oman. To the north, a much more complex pattern appears due to interposition and interactions of multiple wave fronts propagating to the shorelines. Shallower water near the CB also affects south-north tsunami propagation.

Table 3. Geological parameters for potential co-seismic tsunami sources in the MSZ

Magnitude (Mw)	Epicenter (Deg.)		Strike (Deg.)	Dip (Deg.)	Rake (Deg.)	Depth (km)
9.1	24.76 N	64.00 E (FM)	255	3	90	25
9.1	24.75 N	59.72 E (FM)	282	3	90	25
8.7	24.74 N	59.72 E (WM)	282	3	90	25
8.7	24.76 N	64.00 E (EM)	255	3	90	25
8.3	24.74 N	59.72 E (WM)	275	3	90	25
8.3	24.76 N	64.00 E (EM)	258	3	90	25
8.0	24.74 N	59.72 E (WM)	276	3	90	25
8.0	24.76 N	64.00 E (EM)	268	3	90	25
7.5	24.74 N	59.72 E (WM)	277	3	90	25
7.5	24.76 N	64.00 E (EM)	268	3	90	25

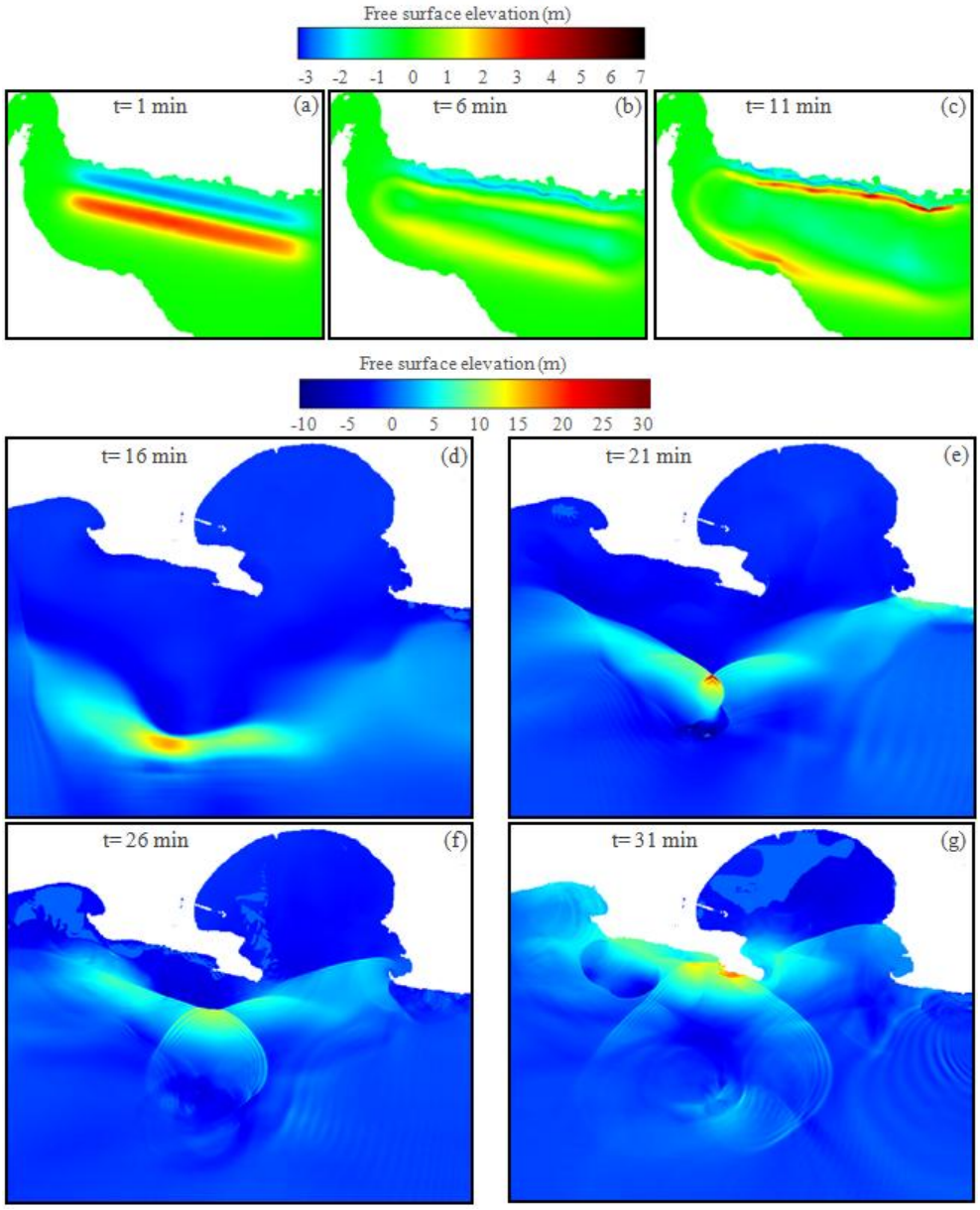

Figure 3. Snapshots of global and local tsunami simulations at times t = 1, 6, 11, 16, 21, 26, and 31 min due to a M_w 9.1 earthquake

Fig. 3 shows four snapshots of instantaneous surface elevation, of the "worst case scenario" Mw 9.1 tsunami source computed in Table 2, after 16 minutes, 21 minutes (time when reaching the underwater mound), 26 minutes (time after passing the underwater mound) and 31 minutes (time when reaching coasts), respectively. We see an initial strong northward directionality of the highest tsunami waves, towards the CB. Once waves reach the shallower continental shelf, they start wrapping up around the bathymetric contours due to refraction (Fig. 3-b).

A characteristic initial tsunami amplitude which is defined as the minimum or maximum elevation found from the bottom co-seismic displacement (maximum uplift and subsidence of the ocean surface) grow with the increase of earthquake magnitude in different scenarios as shown in Table 2. As illustrated in Fig. 3 , about the +8.43 m uplift and -5.86 m subsidence are observed on the water surface elevation immediately after the vibration associated with M_w 9.1. The result shows the trough of tsunami's initial wave is created north of the faulted area and so falling water is first observed along the coastlines locating north of the tsunami source, i.e. Iran and Pakistan. Therefore, the local communities of Iran can benefit it as a useful natural warning sign and can be aware of tsunami acuurence before the arrival of destructive waves. Model results displays that the wavelength of tsunami's initial wave is exactly equal to to the fault width, hence, the width of rupture area in one of the important factor that can change the shape of tsunami wave.

Fig. 3 illustrates tsunami waves damping after the generation of initial wave at the beginning of propagation process, but waves amplify again during approaching to the the coasts because of shoaling

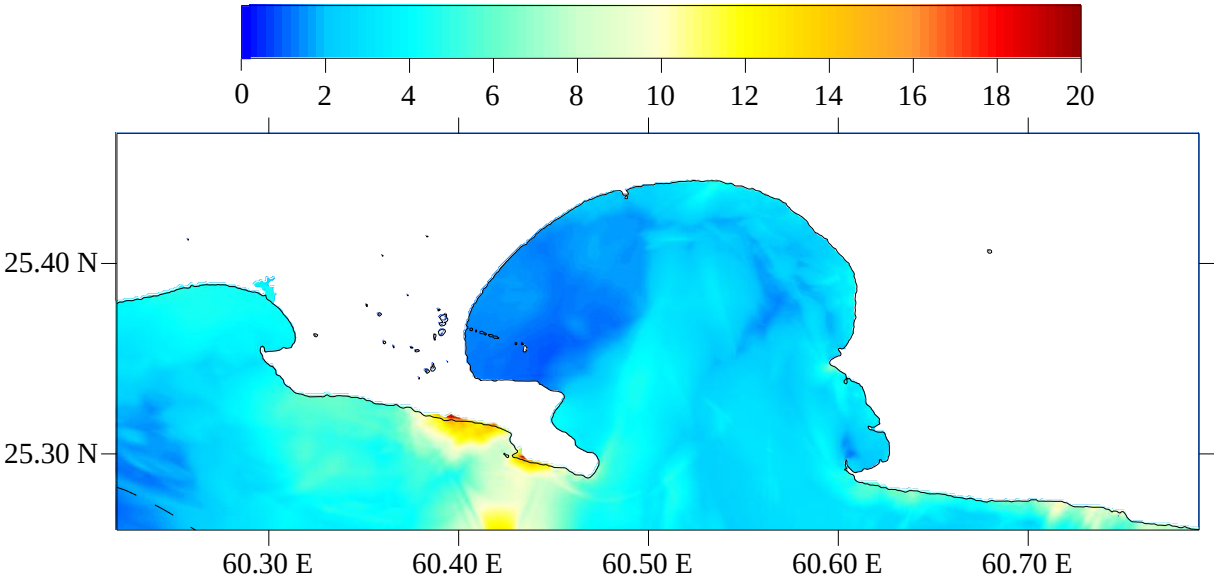

Figure 4. Maximum wave height distribution for M_w 9.1 (upper) and 8.7 (lower) earthquake scenarios

effects. Results show that the generated tsunami waves propagate perpendicular to the fault area, so tsunami waves are mainly just observed at the coasts acrosss from the fault area and the farther latitudainal regions are safe from probable tsunami. Fig. 4 showes the maximum surface elevation computed for M_w 9.1 and 8.7 tsunami sources at any time during the tsunami propagation. We see that waves on the order of at least 22 m (for M_w 9.1) and 8 m (for M_w 8.7) elevation reach the coast. Fig. 4 illustrates the complicated interactions between a tsunami and a harbour through the numerical simulation results. The characteristics of tsunami behaviour are as follows: (1) The tsunami height in the port is not reduced by the bay entrance as the cross-section area of the open section of bay is not small enough. (2) Although the tsunami height in the port varies relatively smoothly, the effect of reflection can be observed in the results. (3) High tsunami waves may appear at a closed-off section surrounding quays and other structures. (4) A tsunami propagating into the port causes high speed wave celerity locally, not only around the coastal lines but in some areas such as a locally-shallow part.

Fig. 5 shows the distribution of maximum computed tsunami height at the various stations of Makran coasts produced by M_w 8-9.1 earthquakes in the western Makran (WM), eastern Makran (EM) and full length of Makran (FM) tsunamigenic sub-regions.

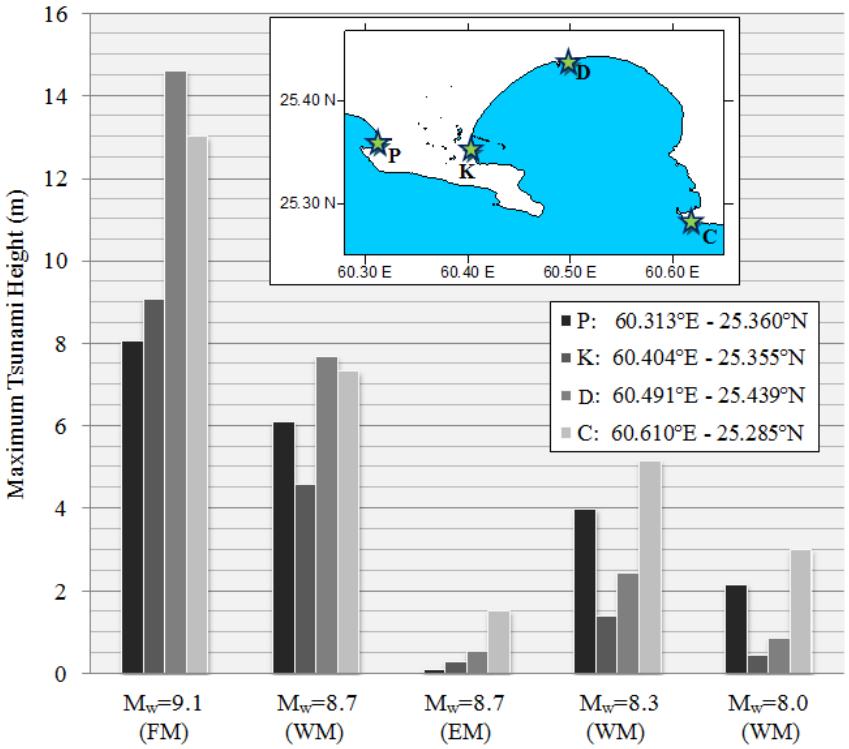

Figure 5. Distribution of maximum computed tsunami height at the various stations of Makran coasts produced by M_w 8-9.1 earthquakes in the WM, EM and FM tsunamigenic sub-regions

These large waves could inundate a large section of the coast within a few hours, greatly complicating emergency response. The western cape of CB tends to reflect energy away from the inner part of bay so its hazard tends to be smaller to the western of the bay. The results show that the wave height at different stations does not always increase with amplification of the earthquake magnitude. As shown in the Fig. 5, the effect of the WM earthquake for M_w 8.7 scenario is much more than EM one.

Time series computed at the 4 stations are shown in Fig. 6 and Fig. 7 for M_w 8.7 and M_w 9.1 tsunami sources, respectively. The results show that the tsunami would reach the shallower water stations C, P, K and D after 19, 29, 32 and 34 minutes, with a leading wave elevation of 13, 8, 9 and 14 meter, respectively for M_w 9.1 and after 20, 31, 35 and 46 minutes, with a leading wave elevation of 5, 4, 1.5 and 2 meter, respectively for M_w 8.7.

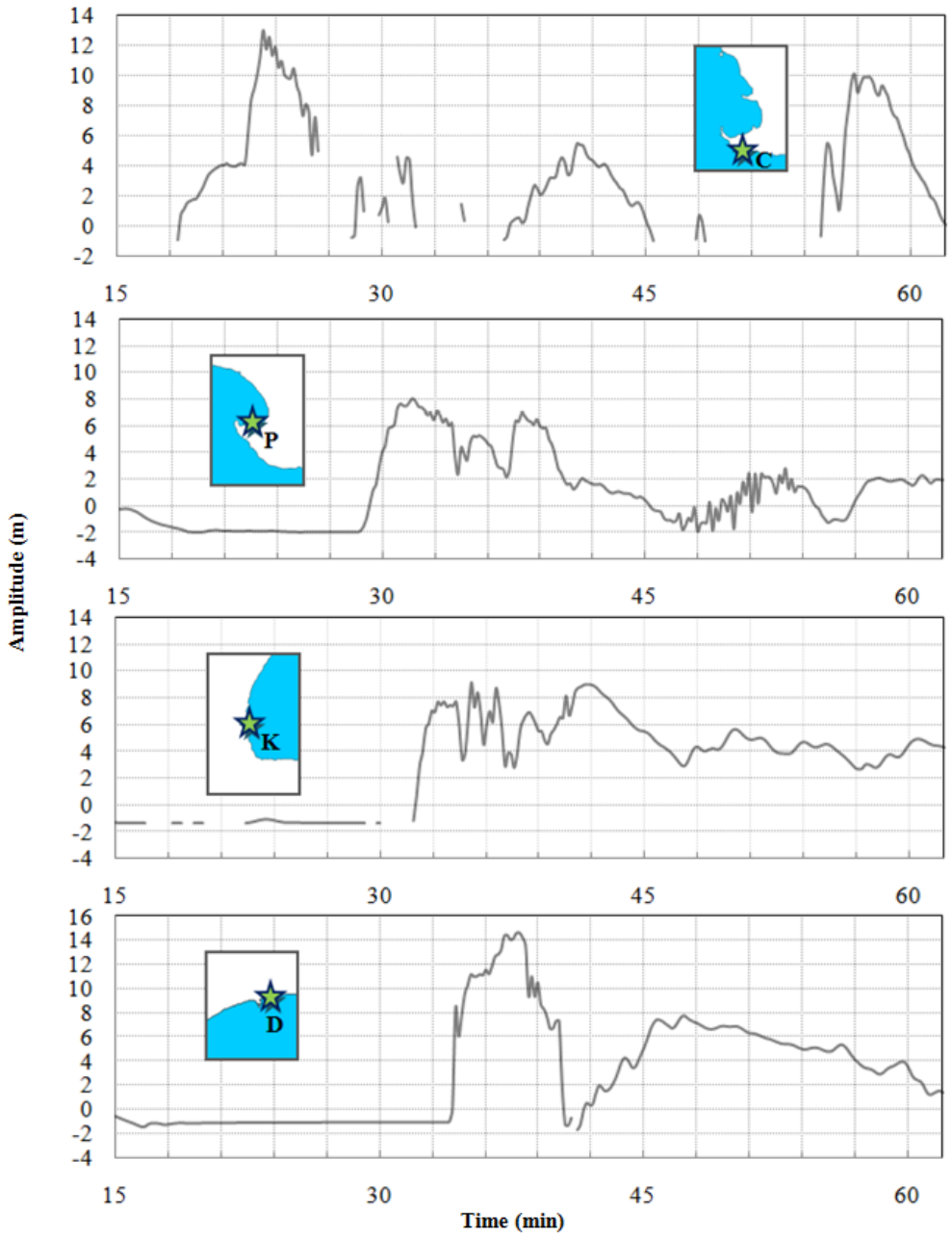

Figure 6. Modeled time series of water surface elevations at various locations along the Makran coast for the M_w 9.1 earthquake tsunami

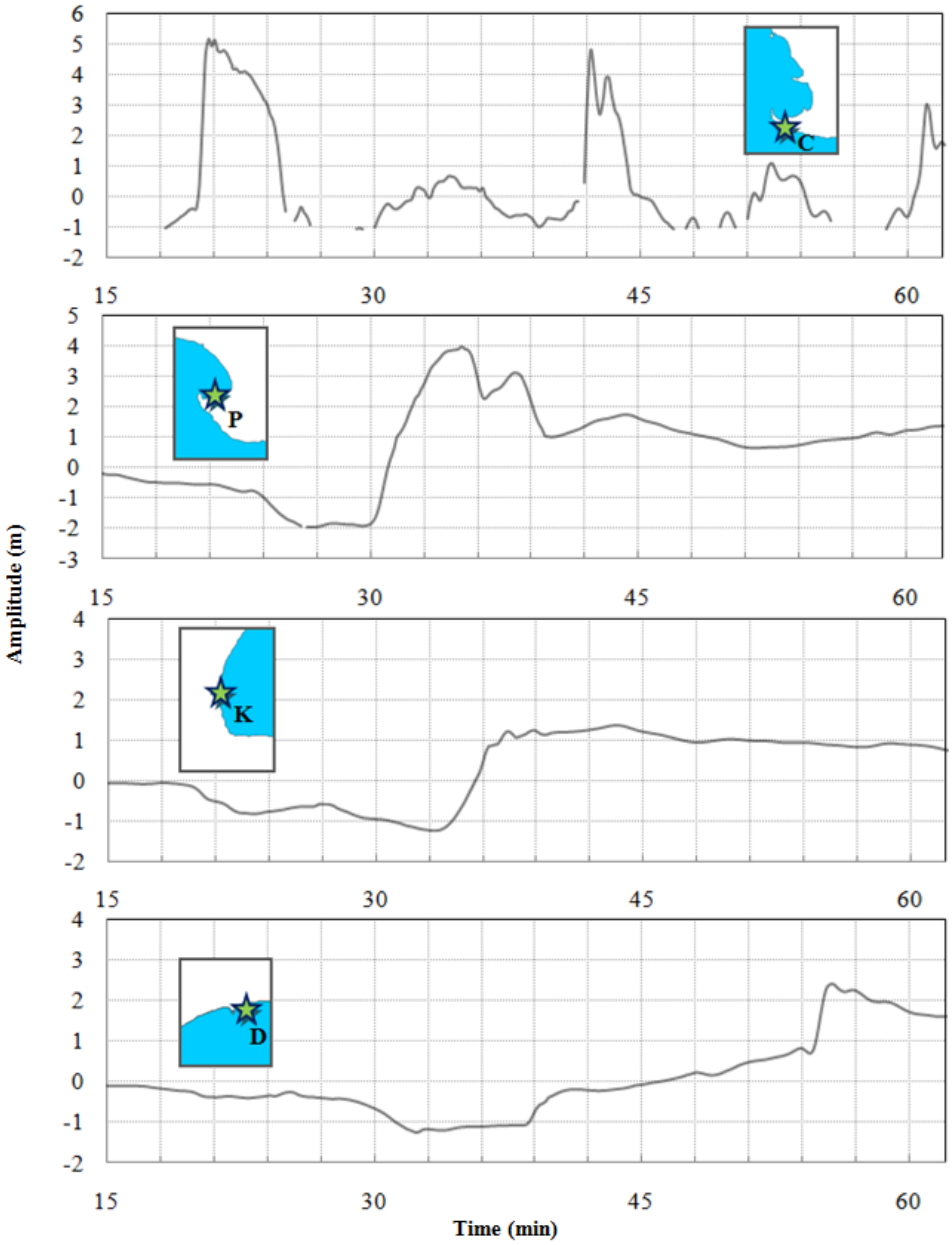

Figure 7. Modeled time series of water surface elevations at various locations along the Makran coast for the M_w 8.7 earthquake tsunami

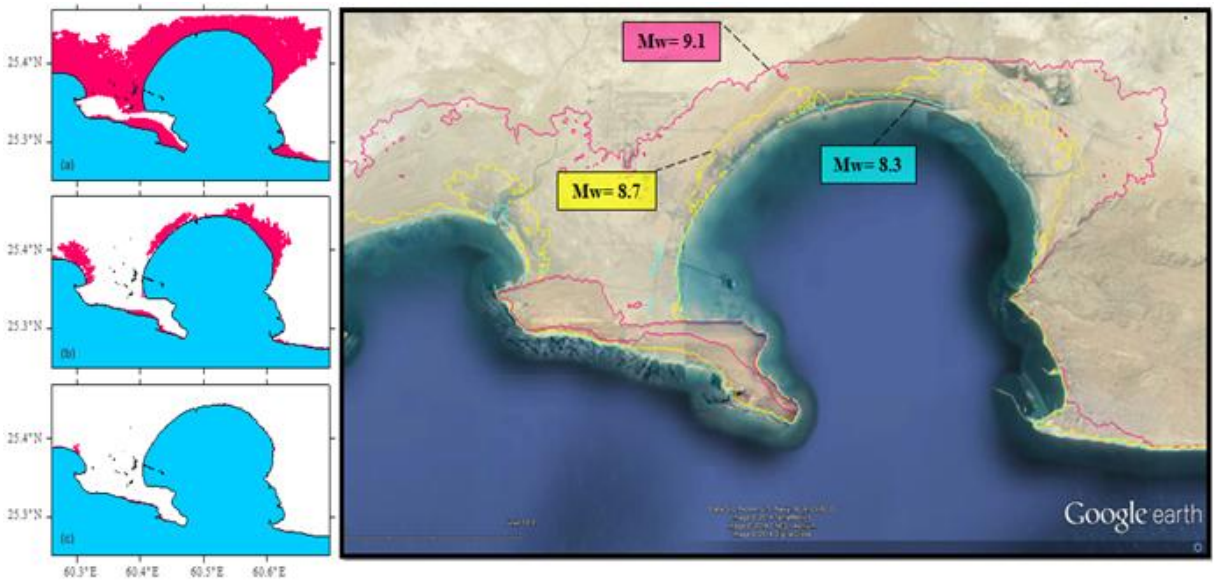

Figure 8. Comparison between flooded area associated with M_w 8.3, 8.7 and 9.1 earthquake scenarios

4.2. Inundation

The following is a list of information outputs based on the procedures described; (1) a listing of all known tsunamigenic events to have impacted CB region; (2) analysis of calculated tsunami propagation patterns for tsunamis from likely earthquake sources to determine potential for impact on Makran coasts; (3) a map showing the coasts most affected with the potential tsunami impact; and (4) the maps for specified tsunami scenarios showing limits of coastal land that is likely to be affected by those scenarios (inundation limits, run-up), water depths at maximum inundation. Tsunami inundation may have a devastating effect on coastal ecosystems. Because of its wide ranging parameters, it may be one of the most difficult to quantify.

Fig. 8 shows the flooded area in CB exerted by earthquake tsunami M_w 8.3, 8.7 and 9.1. Since the tsunami height was not very large, the tsunami running up the land had a less destructive wave force, as can be seen from the picture, but did carry away fishing vessels. Tsunamis flooding the flat port areas can be considered as flows rather than waves, because the incident tsunami is neither a bore-like tsunami nor a broken tsunami wheras the water depth of ports in the entrances of ports is deep. In Fig. 8, there are no structures as obstacles but the existence of structures is replaced by the bottom roughness using the friction coefficients C_d. The friction coefficients have the same values as the conventional tsunami simulation in which it is set to C_d = 0.0025; 0.005; 0.01 for deep water, shallow water and inundation area respectively.

If the water level induced by a tsunami is higher than the height of the ground level of a port, seawater will intrude into the land areas of the port. Since the land area of a port is often low and flat to facilitate cargo-handling, there is a high risk of flooding of wide areas in a short period after the start of inundation.Tsunamis on land may cause not only vessels but also containers, cars and tanks to float and drift. Some of them can hit port facilities and other structures and some will be pulled into the sea by the retreating tsunami. According to the results, the inundation area covered about 12.9, 68.9 and 320.4 km^2 for M_w 8.3, 8.7 and 9.1 respectively at the studying area. Low-lying areas are widespread along the coast of CB and the inundation areas tend to be wide even by lower tsunamis.

5. Conclusions

We applied an integrated modeling strategy and exerted numerical code called GEOWAVE to tsunami generation, propogation and inundation by earthquake. Tsunami features are transferred from the models of Grilli and Watts (1999) and Grilli et al. (2002) into analytical approximations of tsunami sources by TOPICS. This technique constructs an initial condition to treat tsunami generation by coseismic displacement. However, the generality of the modeling framework provided by the model is advantageous in that it automatically covers most of the range of effects, from propagation out of the generation region, through propagation at ocean basin scale, to runup and inundation at affected shorelines. We use a single comprehensive model that adapts automatically to cover each range.

We refined the model grid and the bathymetry/topography to conduct regional case studies, and use the significant capabilities of the Boussinesq wave propagation and inundation model. In these local studies, we use the tsunami source that has been constrained and validated in the present work. The main modeling challenge is to move across a sequence of spatial resolutions needed to resolve wave crests as they move from the deep ocean into complex coastal environments. Refining the model grid towards the coast thus could be done by using nested grids.

We conclude that earthquake tsunami sources are reasonable in our work, because tsunami observations and records are correctly simulated for historical case study. In addition to accurate earthquake tsunami sources from TOPICS, we attribute the successful outcome of our case studies to the inclusion of essential geological data and interpretation, as well as the physical capabilities of the Boussinesq propagation model GEOWAVE. This work demonstrates that the combined software GEOWAVE can produce successful tsunami case studies when provided sufficient geological inputs. However, this study should not be used for flood insurance purposes, because it is not based on a frequency analysis.

Study of natural hazards, such as tsunamis, has a significant deciding role in precise investment, cargo-handling operations and general urban development of CB. The MSZ is indeed the site of large earthquakes with corresponding tsunami generation. Results of numerical simulations performed in this study considering past tsunami occurrence records indicate that the multipurpose Chabahar Port (CP) is expected to experience the tsunami events with heights ranging between 8 to 22 meters. Distances between tectonic sources of tsunami generation and the CP as well as the related earthquake magnitude all affect the tsunami arrival time at the port facilities. Additionally, the bathymetric features have a high bearing on the arrival time and maximum wave height of the tsunami. Wave refraction effects from the coasts and CB, with the latter acting somewhat like a diverging bathymetric lenses on waves, significantly influence the height of such incoming waves. The results are used also to find a best configuration advice for the urban facilities in order to mitigate tsunami related risks, with positioning such facilities at the western cape of the bay would help to reduce any related

untoward ramifications of tsunami inundation on the regional human community.

Using a variety of seismological and tsunami elevation restrictions, a tsunami source made of 9 properly parameterized dislocations sources was developed for the tsunamis associated with MSZ. These sources simulate the co-seismic bottom deformation, caused by the earthquake, that propagated along a 1000 km long rupture zone of the MSZ. The model grid has a 1min by 1min regular mesh, mostly constructed with the ETOPO1 bathymetry and topography (except in coastal region where more accurate data are used). Considering the data available at the present stage, to both construct the model grid and constrain the tsunami source, we believe that we have developed a reasonable ad hoc source for the tsunami events.

We believe that work such as this, in which we achieve a better understanding through modeling of the catastrophic 1945 event, will help the scientific community better predict and mitigate any such future disaster. This will be achieved through a combination of forecasting models with adequate warning systems, and proper education of the local populations.

Acknowledgements

The author thank Dr. Watts and Prof. Grilli for their thoughtful comments in GEOWAVE utilization.

References

1. Akbarpour Jannat M.R., Noranian Esfahani M., Chegini V. and Rezanejad K., 2011 "Hazards Associated with Tsunami Waves in the Gulf of Oman," Journal of Coastal Research SI64:865-869

2. Ambraseys N.N. and Melville C.P., 2005. A history of persian earthquakes. Cambridge University Press, Britain

3. Arthurton R.S., Farah A. and Ahmed W., 1982 "The late cretaceous-cenozoic history of western baluchistan pakistan-the northern margin of the makran subduction complex," Geological Society 10:373-385

4. Berninghausen W.H., 1966 "Tsunamis and Seismic seiches reported from regions adjacent to the Indian Ocean," Bull Seismol Soc Am 56(1):69–74

5. Byrne D., Sykes L.R. and Davis D.M., 1992 "Great thrust earthquakes and aseismic slip along the plate boundary of the Makran subduction zone," Journal Geophys Res 97:449–478

6. Chen Q., Kirby J.T., Dalrymple R.A., Kennedy A.B. and Chawla A., 2000 "Boussinesq modeling of wave transformation, breaking, and runup. II: 2D," Journal Waterway Port Coastal Ocean Eng 126(1): 48–56

7. Day S.J., Watts P., Grilli S.T. and Kirby J.T., 2005 "Mechanical models of the 1975 Kalapana, Hawaii earthquake and tsunami." Mar Geol 215(1–2): 59–92

8. Geist E.L., Titov V.V. and Synolakis C.E., 2006 "Tsunami: Wave of change," Scientific American 56-63, 2006.

9. Grilli S.T. and Watts P., 1999 "Modeling of waves generated by a moving submerged body: Applications to underwater landslides," Engrg Analysis Boundary Elements 23(8):645-656

10. Grilli S.T., Vogelmann S. and Watts P., 2002 "Development of a 3D numerical wave tank for modeling tsunami generation by underwater landslides," Engng Anal Bound Elem 26: 301—313.

11. Grilli S.T., Ioualalen M., Asavanant J., Shi F., Kirby J.T. and Watts P., 2007 "Source Constraints and Model Simulation of the December 26, 2004, Indian Ocean Tsunami," J. Waterway Port Coastal Ocean Eng 133(6):414-428

12. Heck N.H., 1947. List of seismic sea wave. Bull Seismol Soc Am 37(4):269–286

13. Heidarzadeh M., Dolatshahi P., Hajizadeh Zaker N. and Yalciner A.C., 2008 "Historical tsunamis in the Makran subduction zone off Southern Coasts of Iran and Pakistan and results of preliminary numerical modeling," Ocean Eng 35:774–786

14. Heidarzadeh M. and Satake K., 2014 "Possible sources of the tsunami observed in the northwestern Indian Ocean following the 2013 September 24 Mw 7.7 Pakistan inland earthquake," Geophys Journal Int. doi:10.1093/gji/ggu297

15. Heidarzadeh M. and Satake K., 2014 "New Insights into the Source of the Makran Tsunami of 27 November 1945 from Tsunami Waveforms and Coastal Deformation Data" Pure and Appl. Geophys. DOI 10.1007/s00024-014-0948-y

16. Ioualalen M., Pelletier J., Watts P. and Regnier M., 2006 "Numerical modeling of the 26th November 1999 Vanuatu tsunami," Journal Geophys Res 111 C06030

17. Kennedy A.B., Chen Q., Kirby J.T. and Dalrymple R.A., 2000 "Boussinesq modeling of wave transformation, breaking, and runup. I: 1D," Journal Waterway Port Coastal Ocean Eng 126(1):39–47

18. Murty T. and Rafiq M., 1991 "A tentative list of tsunamis in the marginal seas of the north indian ocean," Natural Hazards 4:81-83

19. Neetu S. et al., 2011 "Trapped waves of the 27 November 1945 Makran tsunami: observations and numerical modeling," Natural Hazards DOI 10.1007/s11069-011-9854-0

20. Okada Y., 1985. Surface deformation due to shear and tensile faults in a half-space. Bull Seismol Soc Am 75(4):1135–1154

21. Page W.D., Alt J.N., Cluff L.S. and Plafker G., 1979 "Evidence for the recurrence of large magnitude earthquakes along the Makran Coast of Iran and Pakistan," Tectonophysics 52:533–547

22. Pararas-Carayannis G., 2006 "The potential for tsunami generation along the Makran subduction zone in the northern Arabian Sea. Case study: the

earthquake and tsunami of November 28, 1945," Sci Tsunami Hazards 24(5):358–384

23. Payande A.R., Niksokhan M.H. and Naserian H., 2014 "Tsunami hazard assessment of Chabahar bay related to megathrust seismogenic potential of the Makran subduction zone," Nat Haz 74:1-16

24. Rafi Z., Mahmood N., 2010 "Numerical modeling of tsunami inundation for potential earthquake at makran subduction zone - a case study for gwadar coastal area," Pakistan Meteorological Department, Islamabad PMD-45

25. Rajendran C.P., Ramanamurthy M.V., Reddy N.T. and Rajendran K., 2008 "Hazard implications of the late arrival of the 1945 Makran tsunami," CURRENT SCIENCE, 95(12):1739-1743

26. Rastgoftar E., Akbarpour Jannat M.R., Chegini V. and Rostami M., 2012 "Investigation of Chabahar Bay inundation associated with tsunami of Makran subduction zone," 10th International Conference on Coasts, Ports & Marine Structures (ICOPMAS) Tehran Iran

27. Smith G.L., McNeill L.C., Wang K., He J. and Henstock T.J., 2013 "Thermal structure and megathrust seismogenic potential of the Makran subduction zone," Geophys Res Lett. doi:10.1002/grl.50374

28. Titov V.V., Rabinovich A.B., Mofjeld H.O., Thomson R.E., and Gonzalez F.I., 2005 "The global reach of the 26 December 2004Sumatra tsunami," Science 309: 2045–2048

29. Vernant P.h., Nilforoushan F. and Hatzfeld D. et al., 2004 "Present-day crustal deformation and plate kinematics in the middle east constrained by GPS measurements in Iran and Northern Oman," Geophys J Int 157:381–398

30. Wells D.L. and Coppersmith K.J., 1994 "New empirical relationships among magnitude, rupture length, rupture width, rupture area, and surface displacement," Bulletin of the Seismological Society of America 84 (4), 974–1002

31. Watts P., Borrero J.C., Tappin D.R., Bardet J.P. and Grilli S.T., et al., 1999 "Novel simulation technique employed on the 1998 Papua New Guinea tsunami," Proceedings of 22nd General Assembly IUGG Birmingham UK JSS42 Abstract

32. Watts P., Grilli S.T., Kirby J.T., Fryer G.J. and Tappin D.R., 2003 "Landslide tsunami case studies using Boussinesq model and a fully nonlinear tsunami generation model," Nat Hazards Earth Syst Sci 3:391–402

33. Watts P., Ioulalen M., Grilli S.T., Shi F., Kirby J.T., 2005 "Numerical simulation of the December 26, 2004 Indian Ocean tsunami using a higher-order Boussinesq model," Proc 5th Int Conf on Ocean Wave Measurement and Analysis, WAVES 2005 Madrid Spain Paper No. 221

34. Waythomas C.F. and Watts P., 2003 "Numerical simulation of tsunami generation by pyroclastic flow at Aniakchak Volcano, Alaska," Geophys Res Lett 30(14):1751–1755

35. Wei G. and Kirby J.T., 1995 "Time-dependent numerical code for extended Boussinesq equations," J. Waterway Port Coastal Ocean Eng 121(5): 251–261

36. Wei G., Kirby J.T., Grilli S.T. and Subramanya R., 1995 "A fully nonlinear Boussinesq model for free surface waves. Part 1: Highly nonlinear unsteady waves," J. Fluid Mech 294: 71–92.